Introducing Space into MIMO Capacity Calculations

Tony S. Pollock (Contact Author)

Thushara D. Abhayapala,

Rodney A. Kennedy

National ICT Australia,

Research School of Information Sciences and Engineering,

The Australian National University, Canberra, ACT 0200, Australia.

Phone: +61 2 6125 8800,

Facsimile: +61 2 6125 8623,

Email: tony.pollock@anu.edu.au

Abstract

The large spectral efficiencies promised for multiple-input multiple-output (MIMO) wireless fading channels are derived under certain conditions which do not fully take into account the spatial aspects of the channel. Spatial correlation, due to limited angular spread or insufficient antenna spacing, significantly reduces the performance of MIMO systems. In this paper we explore the effects of spatially selective channels on the capacity of MIMO systems via a new capacity expression which is more general and realistic than previous expressions. By including spatial information we derive a closed-form expression for ergodic capacity which uses the physics of signal propagation combined with the statistics of the scattering environment. This expression gives the capacity of a MIMO system in terms of antenna placement and scattering environment and leads to valuable insights into the factors determining capacity for a wide range of scattering models.

Keywords

MIMO systems, wireless, capacity, spatial correlation, multipath channels, non-isotropic scattering

1 Introduction

Multiple-Input Multiple-Output (MIMO) communication systems using multi-antenna arrays simultaneously during transmission and reception have generated significant interest in recent years. Theoretical work of [41] and [13] showed the potential for significant capacity increases in wireless channels utilizing spatial diversity. Consider a system employing n_{T} transmit antennas and n_{R} receive antennas in a narrowband flat fading channel. It was shown in [13] that as $\min(n_{\mathrm{T}}, n_{\mathrm{R}})$ tends to infinity then the capacity of the system grows proportionally to $\min(n_{\mathrm{T}}, n_{\mathrm{R}})$ for fixed transmit power, provided that the fading between antennas is independent and identically distributed (i.i.d.) Rayleigh. This linear capacity growth has emerged as one of the most promising solutions for overcoming the demand for higher bit rates in wireless communications. In reality, however, the capacity is significantly reduced when the fades are not independent, but correlated due to insufficient antenna separation or angular spread of the scatterers surrounding the arrays [13, 38].

A significant hurdle in analyzing the capacity of wireless fading MIMO systems is the random nature of the channel. The ergodic, or mean, capacity is often used to characterize the random channel capacity. However, the ergodic calculation requires extensive simulations which limits analysis into the physical factors determining MIMO capacity. A closed form expression for the ergodic capacity is derived in [42] for the special case of uncorrelated Rayleigh fading. However, as mentioned above, i.i.d. Rayleigh fading models an unrealistic environment not often seen in practice.

Capacity results for various correlation models using Monte Carlo simulations are studied in [8, 9, 12, 19, 31, 38], and asymptotic results and bounds on the effects of correlated channels are presented in [6, 19, 27, 31, 37, 38]. However, these simulations, bounds and asymptotic results have been for a limited set of channel realizations and/or antenna configurations. For single antenna systems it is sufficient to only consider received signal power and/or the time varying amplitude distribution of the channel. However, for systems employing multiple

antennas, consideration must also be given to the angle of arrival (AOA) of the impinging signals as well as the spatial geometry of the array. Most channel models do not include spatial information (antenna locations and scattering environment) explicitly. Although spatial information is represented by the correlation between channel matrix elements there is no direct realizable physical representation, and, therefore does not easily lend itself to insightful capacity results. In particular, of interest is the effect on channel capacity of antenna placement, particularly in the realistic case when antenna arrays are restricted in size, along with non-isotropic scattering environments.

In contrast, the contribution of this paper is an expression for MIMO capacity which overcomes these limitations, that is, with additional theory for modelling scattering environments which we refine here, we derive a model which can be readily reconciled with a multitude of scattering distributions and antenna configurations and allows us to derive a closed form expression for the MIMO capacity.

In this paper, we exploit the convergence of ergodic capacity as the number of transmit antennas is increased to derive a closed-form channel capacity expression which depends on the correlation between the receive antennas. To model the correlation we generalize the *one-ring* model [24, 38], to develop a closed form expression which depends on the antenna spacing and placement along with the mean angle-of-arrival (AOA) and angular spread for a wide range of common scattering distributions. This allows for a capacity expression which can be evaluated for any general spatial scenario, giving significant insights into the capacity of such systems, without the need for multiple correlation models or extensive simulations.

The remainder of this paper is organized as follows. In Section 2, we derive a closed form expression for the ergodic capacity of a MIMO system and discuss limitations to capacity scaling. In Section 3, we develop a generalized 3D multipath channel model which includes antenna locations and environmental factors to characterize the MIMO wireless channel. Using this model, a closed-form spatial correlation expression for general scattering environments is derived, and we summarize some common scattering distributions. MIMO capacity

is then analyzed in Section 4 for a variety of physically realistic spatial scenarios, and spatial limitations to capacity growth are discussed. Finally, we make some concluding remarks in Section 5.

2 Convergence of Ergodic Capacity

Consider a MIMO system consisting of n_{T} transmit antenna and n_{R} receive antennas. When the transmitted signal vector is composed of statistically independent equal power components, each with a Gaussian distribution, the ergodic channel capacity was shown to be [13, 41],

$$C_{\mathrm{erg}} = E_{\boldsymbol{H}} \left\{ \log \left| \boldsymbol{I}_{n_{\mathrm{R}}} + \frac{\eta}{n_{\mathrm{T}}} \boldsymbol{H} \boldsymbol{H}^{\dagger} \right| \right\}, \tag{1}$$

where $\boldsymbol{H}$ is the $n_{\mathrm{R}} \times n_{\mathrm{T}}$ random flat fading channel matrix, assumed known at the receiver, and normalized such that $E\left\{|h_{rt}|^2\right\} = 1$, where h_{rt} is the channel gain from the t-th transmitter to the r-th receiver. Note that the logarithm is base 2 and gives the capacity in bits-per-second-per-Hertz (bps/Hz).

Let $\boldsymbol{H} = [\boldsymbol{h}_1\, \boldsymbol{h}_2\, \cdots\, \boldsymbol{h}_{n_{\mathrm{T}}}]$, where $\boldsymbol{h}_t$ is the $n_{\mathrm{R}} \times 1$ complex zero-mean Gaussian vector of channel gains corresponding to the t-th transmit antenna, then the correlation matrix at the receiver is defined as $\boldsymbol{R}_{\mathrm{rx}} \triangleq E\left\{\boldsymbol{h}_t \boldsymbol{h}_t^{\dagger}\right\}$, where the expectation is over all transmitters and channel realizations, then

$$\boldsymbol{R}_{\mathrm{rx}} = \begin{bmatrix} \rho_{11} & \rho_{12} & \cdots & \rho_{1 n_{\mathrm{R}}} \\ \rho_{21} & \rho_{22} & & \\ \vdots & & \ddots & \vdots \\ \rho_{n_{\mathrm{R}} 1} & & \cdots & \rho_{n_{\mathrm{R}} n_{\mathrm{R}}} \end{bmatrix}, \tag{2}$$

with elements $\boldsymbol{R}_{\mathrm{rx}}|_{rr'} = \rho_{rr'}$ corresponding to the spatial correlation between two sensors r and r' at the receiver.

Consider the situation where the transmit array has uncorrelated transmit branches corresponding to independent $\boldsymbol{h}_t$ vectors. This can occur when the transmit antennas are sufficiently separated for a given angular spread of the scatterers surrounding the transmit array. For example, using the correlation expression developed in Section 3, a two dimensional isotropic scattering environment with antennas separated by 0.35λ gives correlation of 0.1. However, for more realistic scattering environments, when the transmitter is usually mounted high above the scatterers, the angular spread is considerably less. For angular spread of 3° the antennas must be separated by around 9λ to achieve the same level of correlation. With sufficient transmit antenna spacing the vectors $\boldsymbol{h}_t$ are independent and the sample correlation matrix, defined as

$$\widehat{\boldsymbol{R}}_{\mathrm{rx}} \triangleq \frac{1}{n_{\mathrm{T}}} \sum_{t=1}^{n_{\mathrm{T}}} \boldsymbol{h}_t \boldsymbol{h}_t^{\dagger}, \tag{3}$$

converges to $\boldsymbol{R}_{\mathrm{rx}}$ for large numbers of transmit antennas ($n_{\mathrm{T}} \to \infty$). Observing that the channel matrix product can be expressed as

$$\boldsymbol{H}\boldsymbol{H}^{\dagger} = \sum_{t=1}^{n_{\mathrm{T}}} \boldsymbol{h}_t \boldsymbol{h}_t^{\dagger}, \tag{4}$$

then for a large number of sufficiently separated transmit antennas the ergodic capacity converges to the capacity C,

$$\lim_{n_{\mathrm{T}} \to \infty} C_{\mathrm{erg}} = C \triangleq \log |\boldsymbol{I}_{n_{\mathrm{R}}} + \eta \boldsymbol{R}_{\mathrm{rx}}|. \tag{5}$$

The convergence error of the ergodic capacity to the expression (5) is shown in Fig. 1 for increasing numbers of uncorrelated transmit antennas and various numbers of receiver antennas. It is important to observe that the ergodic capacity approaches the capacity C for finite numbers of transmit antennas, with faster convergence for smaller numbers of receive antennas. Therefore, the capacity expression will be accurate for many practical fixed wireless scenarios, where the receiver has a small number of antennas whilst the base station

is less restricted in geometrical size and is able to provide a sufficient number of uncorrelated transmit branches. Therefore, provided the channel does not contain keyholes[1] and the transmit antennas are sufficient in number and separation, the capacity C provides a good estimate of the ergodic capacity C_{erg}. Note that a bound similar to (5) has also been derived in [2] to demonstrate a space-time cross-correlation model for a von-Mises scattering environment.

[Figure 1 about here.]

2.1 Capacity Scaling Limits

The capacity given by (5) is maximized when there is no correlation between the receive antennas, i.e., $\boldsymbol{R}_{\text{rx}} = \boldsymbol{I}_{n_{\text{R}}}$, giving

$$C_{\max} = n_{\text{R}} \log(1 + \eta). \tag{6}$$

Therefore, in the idealistic situation of zero correlation at both transmitter and receiver arrays (corresponding to the i.i.d. case) we see the maximum capacity scaling is linear in the number of receive antennas. In this case, the system achieves the equivalent of n_{R} independent nonfading subchannels, each with SNR η. This result agrees with the traditional capacity formulation [42] which is widely used to advocate the use of MIMO systems.

Conversely, when each pair of antenna elements at the receiver are fully correlated, the correlation matrix becomes the $n_{\text{R}} \times n_{\text{R}}$ matrix of ones, $\boldsymbol{R}_{\text{rx}} = \mathbf{1}_{n_{\text{R}}}$, and the capacity of the MIMO system will be minimized to

$$C_{\min} = \log(1 + n_{\text{R}}\eta). \tag{7}$$

[1]It has been shown theoretically that some channels may exhibit low capacity even though there is no spatial correlation at the transmitter or receiver [7, 15]. However, no observations of keyhole (pinhole) degenerate channel effects from practical measurements have appeared in the literature. Therefore, in this paper we will assume non-degenerate channels only.

Here the logarithmic capacity growth with increasing receiver antennas is due to an effective increase in the average SNR of the single antenna case, due to the assumption of independent noise at each receiver, and is widely known as a receiver diversity array gain effect.

The capacity (5) provides an expression for the ergodic capacity without the need for extensive simulations. In contrast to current simulation studies presented in the literature, which are difficult to relate to physical factors of the system, in the next section it is shown that for essentially all common scattering distributions, and any array configurations, it is possible to compute a closed form capacity expression.

3 Receiver Spatial Correlation for General Distributions of Farfield Scatterers

3.1 Channel Model

The *one-ring* model was initially proposed in [24] to model fixed wireless communications systems where the base station is elevated and not obstructed by local scattering, whilst the user is uniformly surrounded by scatterers. In [38] this model was extended to include multiple transmit and receive antennas, and the capacity was studied for various transmit angular spreads and receive antenna geometries. In this paper we model the multipath propagation and fading correlation using a generalized 3D *one-ring* model that allows for more general scattering environments at both the transmit and receive arrays. This model allows for greater insights into the spatial factors determining channel capacity, in particular, closed-form capacity expressions can be computed for a wide range of scattering environments and antenna geometries.

Consider the narrowband transmission of n_{T} statistically independent uniform power signals $\{x_1, x_2, \ldots, x_{n_{\mathrm{T}}}\}$ through a general 3D flat fading scattering environment with scatterers assumed distributed in the farfield from the receiver antennas, as shown in Fig. 2, then the

incoming signal from direction $\widehat{\boldsymbol{\psi}}$ at the receiver is given by

$$\Phi(\widehat{\boldsymbol{\psi}}) = \sum_{t=1}^{n_{\mathrm{T}}} x_t \, g_t(\widehat{\boldsymbol{\psi}}) \tag{8}$$

where $k = 2\pi/\lambda$ is the wavenumber with λ the wavelength, and $g_t(\widehat{\boldsymbol{\psi}})$ is the effective random complex gain of the scatters for the transmitted signal x_t from the t-th transmit antenna arriving at the receiver array from direction $\widehat{\boldsymbol{\psi}}$. Since the scatterers are assumed farfield to the receiver antennas, signals impinging on the receiver array will be plane waves, therefore, the received signal at the r-th sensor located at $\boldsymbol{y}_r$ is given by

$$\begin{aligned} z_r &= \int_{\Omega} \Phi(\widehat{\boldsymbol{\psi}}) e^{-ik\boldsymbol{y}_r \cdot \widehat{\boldsymbol{\psi}}} d\Omega(\widehat{\boldsymbol{\psi}}) \\ &= \sum_{t=1}^{n_{\mathrm{T}}} x_t \int_{\Omega} g_t(\widehat{\boldsymbol{\psi}}) e^{-ik\boldsymbol{y}_r \cdot \widehat{\boldsymbol{\psi}}} d\Omega(\widehat{\boldsymbol{\psi}}) \end{aligned} \tag{9}$$

where $d\Omega(\widehat{\boldsymbol{\psi}})$ is a surface element of the unit sphere Ω. Therefore, the channel gain h_{rt} from the t-th antenna to the r-th receiver is given by

$$h_{rt} = \int_{\Omega} g_t(\widehat{\boldsymbol{\psi}}) e^{-ik\boldsymbol{y}_r \cdot \widehat{\boldsymbol{\psi}}} d\Omega(\widehat{\boldsymbol{\psi}}), \tag{10}$$

with normalization $\int_{\Omega} E\left\{|g_t(\widehat{\boldsymbol{\psi}})|^2\right\} d\Omega(\widehat{\boldsymbol{\psi}}) = 1$.

[Figure 2 about here.]

3.2 Correlation of the Received Complex Envelopes

Define the normalized spatial correlation function between the complex envelopes of two received signals r and r' located at positions $\boldsymbol{y}_r$ and $\boldsymbol{y}_{r'}$, respectively, as

$$\rho_{rr'} = \frac{E\left\{z_r \overline{z_{r'}}\right\}}{\sqrt{E\left\{z_r \overline{z_r}\right\} E\left\{z_{r'} \overline{z_{r'}}\right\}}}, \tag{11}$$

where $\overline{x}$ denotes the complex conjugate of x, and z_r denotes the noiseless received signal at receiver r.

From (9) the covariance between signals at sensors r and r' is given by

$$\begin{aligned} E\left\{z_r\overline{z_{r'}}\right\} &= E\left\{\sum_{t=1}^{n_{\mathrm{T}}} x_t \int_\Omega g_t(\widehat{\boldsymbol{\psi}})e^{-ik\boldsymbol{y}_r\cdot\widehat{\boldsymbol{\psi}}}d\Omega(\widehat{\boldsymbol{\psi}})\sum_{t'=1}^{n_{\mathrm{T}}}\overline{x_{t'}}\int_\Omega \overline{g_{t'}(\widehat{\boldsymbol{\psi}}')}e^{ik\boldsymbol{y}_{r'}\cdot\widehat{\boldsymbol{\psi}}'}d\Omega(\widehat{\boldsymbol{\psi}}')\right\} \\ &= \sigma_{\mathrm{T}}^2\int_\Omega\sum_{t=1}^{n_{\mathrm{T}}} E\left\{g_t(\widehat{\boldsymbol{\psi}})\overline{g_t(\widehat{\boldsymbol{\psi}}')}\right\}e^{-ik(\boldsymbol{y}_r\cdot\widehat{\boldsymbol{\psi}}-\boldsymbol{y}_{r'}\cdot\widehat{\boldsymbol{\psi}}')}d\Omega(\widehat{\boldsymbol{\psi}})d\Omega(\widehat{\boldsymbol{\psi}}') \end{aligned} \tag{12}$$

where $\sigma_{\mathrm{T}}^2 = E\left\{|x_t|^2\right\}, \forall t$, is the transmit power for each antenna, and it is assumed the transmitted symbols are independent across antennas and independent of the scattering environment. Assuming a zero-mean uncorrelated scattering environment, the scattering channel is characterized by the second-order statistics of the scattering gain function $g_t(\widehat{\boldsymbol{\psi}})$, given by,

$$E\left\{g_t(\widehat{\boldsymbol{\psi}})\overline{g_t(\widehat{\boldsymbol{\psi}}')}\right\} = G_t(\widehat{\boldsymbol{\psi}})\delta(\widehat{\boldsymbol{\psi}}-\widehat{\boldsymbol{\psi}}'), \tag{13}$$

where $G_t(\widehat{\boldsymbol{\psi}}) = E\left\{|g_t(\widehat{\boldsymbol{\psi}})|^2\right\}$, then (12) simplifies to

$$E\left\{z_r\overline{z_{r'}}\right\} = \sigma_{\mathrm{T}}^2\int_\Omega\sum_{t=1}^{n_{\mathrm{T}}} G_t(\widehat{\boldsymbol{\psi}})e^{-ik(\boldsymbol{y}_r-\boldsymbol{y}_{r'})\cdot\widehat{\boldsymbol{\psi}}}d\Omega(\widehat{\boldsymbol{\psi}}). \tag{14}$$

Substitution of (14) into (11) gives the correlation between the two receiver sensors as

$$\rho_{rr'} = \int_\Omega \mathcal{P}(\widehat{\boldsymbol{\psi}})e^{-ik(\boldsymbol{y}_r-\boldsymbol{y}_{r'})\cdot\widehat{\boldsymbol{\psi}}}d\Omega(\widehat{\boldsymbol{\psi}}), \tag{15}$$

where $\mathcal{P}(\widehat{\boldsymbol{\psi}})$ is the normalized average power received from direction $\widehat{\boldsymbol{\psi}}$, defined by

$$\mathcal{P}(\widehat{\boldsymbol{\psi}}) \triangleq \frac{\sum_{t=1}^{n_{\mathrm{T}}} G_t(\widehat{\boldsymbol{\psi}})}{\int_\Omega\sum_{t=1}^{n_{\mathrm{T}}} G_t(\widehat{\boldsymbol{\psi}})d\Omega(\widehat{\boldsymbol{\psi}})}. \tag{16}$$

In two dimensional scattering environments the power distribution (16) is commonly known as the power azimuth spectrum (PAS) [23], or power azimuth distribution (PAD) [18].

To highlight the factors which effect spatial correlation the Jacobi-Anger plane wave expansion is employed [10],

$$e^{ik\boldsymbol{y}\cdot\widehat{\boldsymbol{\psi}}} = \sum_{m=0}^{\infty} i^m (2m+1) j_m(k\|\boldsymbol{y}\|) P_m(\cos\xi), \tag{17}$$

where $\xi = \angle(\boldsymbol{y}, \widehat{\boldsymbol{\psi}})$ denotes the angle between $\boldsymbol{y}$ and $\widehat{\boldsymbol{\psi}}$, $j_m(\cdot)$ are the spherical Bessel functions of the first kind, and $P_m(\cdot)$ are the Legendre polynomials of degree m. To further separate the effects of the scattering and the sensor positioning, consider the identity [4, p.694]

$$P_m(\cos\xi) = \frac{4\pi}{2m+1} \sum_{n=-m}^{m} \overline{Y_m^n(\widehat{\boldsymbol{y}})} Y_m^n(\widehat{\boldsymbol{\psi}}), \tag{18}$$

where $\widehat{\boldsymbol{y}} = \boldsymbol{y}/\|\boldsymbol{y}\|$ and $Y_m^n(\cdot)$ represent spherical harmonics [10, p.25], then the spatial correlation (15) can be expressed as

$$\rho_{rr'} = 4\pi \sum_{m=0}^{\infty} \sum_{n=-m}^{m} (-i)^m \alpha_m^n \, j_m(k\|\boldsymbol{y}_r - \boldsymbol{y}_{r'}\|) Y_m^n \left(\frac{\boldsymbol{y}_{r'} - \boldsymbol{y}_r}{\|\boldsymbol{y}_r - \boldsymbol{y}_{r'}\|} \right), \tag{19}$$

where coefficients α_m^n characterize the scattering environment,

$$\alpha_m^n = \int_{\Omega} \mathcal{P}(\widehat{\boldsymbol{\psi}}) \overline{Y_m^n(\widehat{\boldsymbol{\psi}})} d\Omega(\widehat{\boldsymbol{\psi}}), \tag{20}$$

and are independent of the antenna positions. The spatial correlation (19) is now composed of a summation of terms, where each term has independent factors characterizing the scattering environment and the antenna locations. Therefore, unlike previous models, where the antenna locations and the scattering environment are coupled, the separate effects of antenna geometry and scattering environment on the channel capacity can now be studied.

3.2.1 Isotropic Scattering Environment

For the special case of isotropic scattering (omnidirectional diffuse fields) the power distribution is given by the constants, $\mathcal{P}(\widehat{\boldsymbol{\psi}}) = 1/2\pi^2$ and $\mathcal{P}(\psi) = 1/2\pi$, for the 3D and 2D scattering

environments respectively[2]. In this case, the summation in (19) reduces to a single term and the 3D and 2D spatial correlation can be shown to be:

$$\rho_{rr'}^{\mathrm{3D}} = j_0(k\|\boldsymbol{y}_r - \boldsymbol{y}_{r'}\|), \tag{21}$$

$$\rho_{rr'}^{\mathrm{2D}} = J_0(k\|\boldsymbol{y}_r - \boldsymbol{y}_{r'}\|), \tag{22}$$

which agree with the classical results [11, 20], where $J_n(\cdot)$ are the Bessel functions of order n, and by definition $j_0(\cdot) = \mathrm{sinc}(\cdot)$. With these analytic forms for the spatial correlation we can compute the capacity (5). Figure 3 shows the theoretical capacity for increasing antenna numbers for a fixed aperture uniform linear (ULA) and circular (UCA) arrays in 2D and 3D isotropic scattering with SNR of 10dB. It is clear from comparison of the 2D and 3D capacities that any elevation spread has little effect on the capacity of an array in the horizontal plane. This can be seen in the insert of Fig. 3 where the spatial correlation for increasing spatial separation is shown for the 2D and 3D isotropic scattering environments, here the two functions $J_0(\cdot)$ and $j_0(\cdot)$ are qualitatively similar, particularly for low spatial separation. Therefore, without loss of generality, we focus on scattering environments where there is negligible power arriving from elevation angles.

[Figure 3 about here.]

3.3 Two Dimensional Scattering Environment

Consider a 2D scattering environment where the signals arrive only from the azimuthal plane, then $\boldsymbol{y} = (\|\boldsymbol{y}\|, \theta_y)$ and $\widehat{\boldsymbol{\psi}} = (1, \psi)$ in polar coordinates, and (17) can be shown to reduce to,

$$\begin{aligned} e^{ik\boldsymbol{y}\cdot\widehat{\boldsymbol{\psi}}} &= J_0(k\|\boldsymbol{y}\|) + 2\sum_{m=1}^{\infty} i^m J_m(k\|\boldsymbol{y}\|)\cos(m\xi) \\ &= \sum_{m=-\infty}^{\infty} J_m(k\|\boldsymbol{y}\|)e^{-im(\theta_y - \pi/2)}e^{im\psi}. \end{aligned} \tag{23}$$

[2]The 2D scattering environment is a special case of the 3D case when the signals arrive from the azimuthal plane only.

Substitution of (23) into (15) gives the spatial correlation for a 2D environment as

$$\rho_{rr'} = \sum_{m=-\infty}^{\infty} \alpha_m J_m(k\|\boldsymbol{y}_r - \boldsymbol{y}_{r'}\|)e^{im\theta_{rr'}}, \tag{24}$$

where $\theta_{rr'}$ is the angle of the vector connecting $\boldsymbol{y}_r$ and $\boldsymbol{y}_{r'}$. The coefficients α_m characterize any possible 2D scattering environment surrounding the receiver and are given by

$$\alpha_m = \int_0^{2\pi} \mathcal{P}(\psi)e^{-im\psi}d\psi, \tag{25}$$

where $\mathcal{P}(\psi)$ is the average angular power distribution, or power azimuth distribution (PAD).

Bessel functions $J_n(x), |n| > 0$ exhibit spatially high pass behavior, that is, for fixed order n, $J_n(x)$ starts small and becomes significant for arguments $x \approx \mathcal{O}(n)$. Therefore, to compute the spatial correlation for points closely located in space, only a few terms in the sum (24) need to be evaluated in order to give a very good approximation [21]. Thus, closed-form solutions for the correlation can be found provided closed-form expressions exist for the scattering coefficients (25). As summarized next, for many common scattering distributions, there exists closed-form expressions for the scattering coefficients α_m and thus the capacity can be computed for a wide range of realistic scattering environments.

3.4 Non-isotropic Scattering Environments

The spatial correlation as a function of receive antenna separation depends on the scattering distribution surrounding the receiver. One of the most commonly used distributions is the isotropic scattering model, where the power is assumed to be uniform over all AOA [20]. However, as discussed in [5, 29, 30, 35], and verified via experimental measurement campaigns [14, 25, 26, 34, 39, 45], many realistic scattering environments have nonuniform AOA distributions.

Non-isotropic scattering distributions model multipath as energy arriving from a particular direction with angular spread related to the non-isotropy parameter of the distribution, as shown in Fig. 4. The non-isotropic distributions are characterized by the mean

AOA ψ_o and the angular spread σ, defined as the standard deviation of the distribution. Several distributions have been proposed for modelling the non-isotropic scattering environment [1,22,32,36,39,44], in the following we outline several common distributions along with the scattering parameter effects on spatial correlation and capacity.

[Figure 4 about here.]

3.4.1 Uniform Limited Distributed Field

When the energy arrives uniformly from a restricted range of azimuth angles $\pm\Delta$ around a mean AOA, $\psi_0 \in [-\pi, \pi)$, we have the uniform limited distribution,

$$\mathcal{P}(\psi) = \begin{cases} K_{\mathrm{U}}, & |\psi - \psi_0| \leq \Delta \\ 0, & \text{elsewhere} \end{cases}, \tag{26}$$

where K_{U} is a normalization constant such that $\int_0^{2\pi} \mathcal{P}(\psi) d\psi = 1$. In this case $K_{\mathrm{U}} = 1/2\Delta$ and the scattering environment coefficients (25) are given by,

$$\alpha_m = \frac{\sin(m\Delta)}{m\Delta} e^{-im\psi_0}, \tag{27}$$

which gives the equivalent correlation expression to that derived in [36]. For $\Delta = \pi$ (isotropic scattering) (24) is given by a single term, and the correlation coefficient becomes $J_0(k\|\boldsymbol{y}_r - \boldsymbol{y}_{r'}\|)$, which agrees with earlier results.

3.4.2 Truncated Gaussian Distributed Field

The Gaussian distribution was proposed in [22] for modelling the distribution of scatterers as

$$\mathcal{P}(\psi) = K_{\mathrm{G}} e^{-\left(\frac{\psi - \psi_0}{\sqrt{2}\sigma_{\mathrm{G}}}\right)^2}, \qquad \psi \in [-\pi, \pi) \tag{28}$$

where σ_{G} is the standard deviation of the non-truncated distribution and is related to the angular spread. K_{G} is a normalization constant, which can be shown to be

$$K_{\mathrm{G}} = \frac{1}{\sqrt{2\pi}\sigma_{\mathrm{G}} \mathrm{erf}(\pi/\sqrt{2}\sigma_{\mathrm{G}})}, \tag{29}$$

where $\mathrm{erf}(x)$ is the error function, defined as $\mathrm{erf}(x) = \int_0^x e^{-t^2} dt$. In this case (25) is given by

$$\alpha_m = \frac{\Re\left\{\mathrm{erf}\left(\frac{\pi/2 + im\sigma_{\mathrm{G}}^2}{\sqrt{2}\sigma_{\mathrm{G}}}\right)\right\}}{\mathrm{erf}\left(\frac{\pi}{\sqrt{2}\sigma_{\mathrm{G}}}\right) e^{m^2\sigma_{\mathrm{G}}/2}} e^{-im\psi_0}, \tag{30}$$

which is well approximated by $\alpha_m \approx e^{-m^2\sigma_{\mathrm{G}}/2} e^{-im\psi_0}$ for narrow angular spread [40].

3.4.3 Truncated von-Mises Distributed Field

Another recently proposed non-isotropic scattering model is the von-Mises distribution [1],

$$\mathcal{P}(\psi) = K_{\mathrm{v}} e^{\kappa \cos(\psi - \psi_0)}, \qquad \psi \in [-\pi, \pi) \tag{31}$$

where $\kappa \geq 0$ represents the degree of non-isotropy and is related to the angular spread of the AOA. Here the normalization constant K_{v} is given by,

$$K_{\mathrm{v}} = \frac{1}{2\pi I_0(\kappa)}, \tag{32}$$

where $I_m(\cdot)$ is the modified Bessel function of the first kind. For $\kappa = 0$ (isotropic scattering) the distribution becomes $\mathcal{P}(\psi) = 1/2\pi$, while for small angular spread, $\kappa = \infty$, the distribution is the Dirac delta function $\mathcal{P}(\psi) = \delta(\psi - \psi_0)$. For the truncated von-Mises field the scattering environment coefficients are given by

$$\alpha_m = \frac{I_{-m}(\kappa)}{I_0(\kappa)} e^{-im\psi_0}. \tag{33}$$

3.4.4 Truncated Laplacian Distributed Field

For some scenarios the Laplacian distribution has been proposed as a good model of the scattering distribution [32, 39]. The Laplacian distribution is defined as

$$\mathcal{P}(\psi) = K_{\mathrm{L}} e^{-\sqrt{2}|\psi - \psi_0|/\sigma_{\mathrm{L}}}, \qquad \psi \in [-\pi, \pi) \tag{34}$$

where σ_{L} is the standard deviation of the non-truncated distribution and is related to the angular spread of the AOA, and the normalization constant K_{L} is given by

$$K_{\mathrm{L}} = \frac{1}{\sqrt{2}\sigma_{\mathrm{L}}(1 - e^{-\sqrt{2}\pi/\sigma_{\mathrm{L}}})}. \tag{35}$$

Here the scattering coefficients (25) can be expressed as [40],

$$\alpha_m = \frac{(1 - (-1)^{\lceil m/2 \rceil} e^{-\pi/\sqrt{2}\sigma_{\mathrm{L}}} F_m)}{(1 + \sigma_{\mathrm{L}}^2 m^2/2)(1 - e^{-\pi/\sqrt{2}\sigma_{\mathrm{L}}})}, \tag{36}$$

where $F_m = 1$ for even m, and $F_m = m\sigma/\sqrt{2}$ for odd m. In this case, the correlation agrees with the recent derivation in [43], where the spatial correlation is derived for a uniform circular array within a Laplacian distribution scattering environment.

The above distributions are shown in Fig. 5 for various angle spreads $\sigma = \{20°, 30°, 60°\}$ about the mean AOA $\psi_0 = 0$, where the angle spread is defined as the standard deviation of the truncated distribution and is related to the nonisotropy parameter Δ, σ_{G}, κ, or σ_{L}.

[Figure 5 about here.]

We now explore the effects on spatial correlation of angle spread and mean AOA for the above distributions. In order to compare the spatial correlation we set the angle spread to $\sigma = \{1°, 5°, 10°\}$ for each distribution and increase the separation distance between the antennas, located on the x-axis. The spatial correlation for mean AOA $\psi_0 = 90°$ (broadside) is shown in Fig. 6. As shown, the spatial correlation decreases as the antenna spacing and/or the angular spread increases[3]. Here we also see that the scattering models all give similar spatial correlation for the same angular spread, particularly for small spatial separations, indicating that the choice of non-isotropic distribution is unimportant as the distribution variance dominates correlation. However, due to the higher concentration of energy about the mean for the Laplacian distribution[4], for large spatial separation the Laplacian model

[3]It is important to note that the correlation does not decrease monotonically with antenna separation, therefore, in certain scenarios increasing the antenna spacing may actually increase spatial correlation.

[4]when compared with the other models for identical angular spread

generally gives higher correlation than the other three distributions for all angular spreads considered. Finally, we observe that in all cases the von-Mises distribution gives spatial correlation nearly identical to that of the Gaussian model. This agrees with observations made in [1], where it was noted that the von-Mises distribution resembles a Gaussian pdf for large κ (small angular spread) [28, p.61].

[Figure 6 about here.]

In Fig. 7 the spatial correlation is shown for mean AOA $\psi_0 = 30^\circ$ (60° from broadside). Similar results are seen as for the broadside case, however, we see significant increase in spatial correlation for all angle spreads and distributions for the same spatial separation as before. Therefore, due to the reduction of resolvable angular spread at the antennas, the spatial correlation is increased as the mean AOA moves away from the broadside angle, where the broadside angle defined as the angle perpendicular to the line connecting the two antennas.

[Figure 7 about here.]

4 Capacity Results

In this section we study the spatial effects of non-isotropic scattering and antenna geometry on the capacity of MIMO systems. Using (5) and (24) along with the expressions for the non-isotropic scattering coefficients given in the previous section, we compute the capacity bound for a variety scattering environments for the uniform linear (ULA) and uniform circular (UCA) arrays. In particular, of interest is the notion of linear in antenna number capacity scaling widely used to advocate the use of MIMO systems [13, 42], and how this is effected by non-isotropic scattering and dense array configurations. For all scenarios we consider a signal-to-noise ratio of $\eta = 10$dB. For comparison, the maximum (6) and minimum (7)

capacities are also shown, corresponding to no spatial correlation and full spatial correlation capacities, respectively.

First we consider the capacity of an 8 antenna fixed aperture (length/diameter) 3.5λ array for each scattering distribution against the non-isotropy factor and for mean AOA $\psi_0 = \{0°, 45°, 90°\}$. As shown in Fig. 8, the capacity increases for increasing non-isotropy factor for the uniform, Gaussian, and Laplacian distributions, corresponding to an increase in angle spread surrounding the receiver. For the von-Mises distribution, the capacity decreases as κ increases, corresponding to a reduction in angular spread at the receiver. For all distributions, the reduction in capacity with decreasing angular spread is most pronounced for the ULA when the mean AOA is inline with the array ($\psi_0 = 0°$). However, for the UCA the capacity is unaffected by mean AOA, advocating the use of 2D array configurations, which are less sensitive to the mean direction of signal arrival, compared to the 1D linear arrays.

[Figure 8 about here.]

We now consider the capacity scaling of a MIMO system as the number of receive antennas increases whilst the array aperture size remains fixed. First we consider the ULA and UCA of aperture (length/diameter) $D = \{0.4\lambda, 0.6\lambda, 0.8\lambda\}$ in an isotropic scattering environment, shown in Fig. 9.

[Figure 9 about here.]

It can be observed from Fig. 9 that the capacity scales almost linearly with the number of antennas before reducing to logarithmic growth after some saturation point. The saturation point is clearly related to the aperture of the array for both the ULA and UCA, where smaller apertures saturate for lower numbers of receive antennas. The capacity scaling of the ULA and UCA is shown in Fig. 10 and Fig. 11, respectively, for fixed aperture 4λ with angular spread $\sigma = \{1°, 5°, 20°\}$ of the various scattering distributions.

[Figure 10 about here.]

[Figure 11 about here.]

Again, for both ULA and UCA saturation is observed in the capacity scaling, where the growth reduces from approximately linear to logarithmic after the number of antennas reaches a distinct threshold. Note that the array aperture is sufficiently large so any saturation is due to the reduction of angular spread at the receiver, which is clearly seen in both figures.

To emphasis the effects of saturation with antenna numbers seen above, we can write the capacity (5) as

$$C = C_{\max} + \Delta C \tag{37}$$

where $C_{\max}$ is the maximum antenna capacity (6), and $\Delta C = \log|\mathbf{\Gamma}_{\rm rx}|$, where $\mathbf{\Gamma}_{\rm rx}$ is the $n_{\rm R} \times n_{\rm R}$ matrix

$$\mathbf{\Gamma}_{\rm rx} = \begin{bmatrix} 1 & \frac{\eta}{1+\eta}\rho_{12} & \cdots & \frac{\eta}{1+\eta}\rho_{1n_{\rm R}} \\ \frac{\eta}{1+\eta}\rho_{21} & 1 & & \vdots \\ \vdots & & \ddots & \\ \frac{\eta}{1+\eta}\rho_{n_{\rm R}1} & \cdots & & 1 \end{bmatrix}. \tag{38}$$

Note that $\mathbf{\Gamma}_{\rm rx}$ is a positive semi-definite matrix with $0 \leq |\Gamma_{\rm rx}| \leq 1$, thus $\Delta C \leq 0$, therefore ΔC represents the loss of capacity due to antenna correlation at the receiver. The loss of capacity due to correlation is shown in Fig. 12(a) for a ULA for fixed aperture $D = \{0.5\lambda, 1.5\lambda, 2.5\lambda, 3.5\lambda, 4.5\lambda\}$ in an isotropic scattering environment. Here the distinct saturation point in antenna number is clearly visible with increasing aperture. Likewise, the loss in capacity is significant beyond an antenna saturation point for increasing angular spread as shown in Fig. 12(b) for a ULA of fixed aperture 4λ.

[Figure 12 about here.]

Using a singular value decomposition of the channel matrix, the capacity of a MIMO system can be shown to be equivalent to the sum of the capacities of $\min(n_{\rm T}, n_{\rm R})$ subchannels, each with independent power gains corresponding to the eigenvalues of the channel

matrix product $\boldsymbol{H}\boldsymbol{H}^{\dagger}$ [41]. The subchannel gains depend on the correlation between channel branches, and as the correlation increases some subchannels have gains too small to convey information at any significant rate [38]. Therefore, as seen here, as the number of antennas increases for a fixed aperture, or angular spread, due to increased channel branch correlation there exists a saturation point at which the subchannels generated by any addition antennas have negligible gains and do not increase the capacity, other than logarithmic array gain.

This saturation effect has significant implications for realizable MIMO systems, as the saturation point gives the optimal number of antennas required to maximize capacity, after which there are negligible gains. Asymptotic results for the fixed aperture ULA in isotropic scattering are studied in [46], with identical independent results in [17]. However, the saturation point for fixed aperture arrays has not been addressed so far, except for the special case of the UCA [33]. Promising results from a spatial model presented in [3] indicate the throughput of a MIMO system is limited by the radius of the region containing the antenna arrays, agreeing with observations in this paper. Likewise, to the authors' knowledge, no analytical results exist for the capacity scaling saturation due to insufficient angular spreads, although the effect on capacity due to limited angular spread at the transmitter has been reported in [38], and observed elsewhere, e.g. [16], via simulation.

5 Conclusions

In i.i.d. Rayleigh fading channels the capacity of a multi-antenna system has been shown to grow linearly with antenna numbers. However, in realistic propagation environments, the fading is correlated due to insufficient antenna spacing or angular spread, and the capacity is often significantly lower than that predicted for i.i.d. fading. By assuming a sufficient number of sufficiently separated transmit antennas we have derived a closed-form expression for the capacity of a MIMO random fading channel. Using a novel channel model we separate the effects of the scattering environment and antenna array configuration on the spatial

correlation at the receiver, allowing for capacity evaluation of systems for a wide variety of scattering environments and antenna placement.

We show that the angular spread surrounding the receiver dominates the spatial correlation and thus capacity, rather than the choice of scattering distribution. However, this may not hold for multi-modal distributions which were not discussed here, but are fully captured by our analytical framework. For 1D arrays is was observed that the mean AOA has a significant impact on the capacity of the system, advocating the use of 2D arrays, which are less sensitive to the mean direction of signal arrival.

The capacity was also shown to suffer from a saturation effect in the number of antennas for a fixed angular spread or array aperture. This saturation point, at which the capacity scaling is reduced from linear to logarithmic increase with increasing antenna numbers, is an important factor in the design of practical MIMO systems and needs further investigation.

With the improved spatial channel modelling and capacity expressions presented in this paper, it is hoped the spatial factors influencing the capacity of wireless multi-antenna systems can be better exploited to aid in the design of realistic high-capacity/high-quality wireless communication systems.

References

[1] A. Abdi, J.A Barger, and M. Kaveh. A parametric model for the distribution of the angle of arrival and the associated correlation function and power spectrum at the mobile station. *IEEE Transactions on Vehicular Technology*, 51(3):425–434, 2002.

[2] A. Abdi and M. Kaveh. A space-time correlation model for multielement antenna systems in mobile fading channels. *IEEE Journal on Selected Areas in Communications*, 20(3):550–560, 2002.

[3] T.D. Abhayapala, T.S. Pollock, and R.A. Kennedy. Spatial decomposition of MIMO wireless channels. In *Seventh International Symposium on Signal Processing and its Applications*, Paris, France, 2003.

[4] G.B. Arfken, editor. *Mathematical Methods for Physics*. Academic Press, Orlando, FL, 3rd edition, 1985.

[5] W.R. Braun and U. Dersch. A physical mobile radio channel model. *IEEE Transactions on Vehicular Technology*, 40:472–482, 1991.

[6] C. Chen-Nee, D.N.C. Tse, J.M. Kahn, and R.A. Valenzuela. Capacity scaling in MIMO wireless systems under correlated fading. *IEEE Transactions on Information Theory*, 48(3):637–650, 2002.

[7] D. Chizhik, G.J. Foschini, M.J. Gans, and J.M. Kahn. Capacities of multi-antenna transmit and receive antennas: correlation and keyholes. *Electronic Letters*, 36(13):1099–1100, 2000.

[8] D. Chizhik, F. Rashid-Farrokhi, J. Ling, and A. Lozano. Effect of antenna separation on the capacity of blast in correlated channels. *IEEE Communications Letters*, 4(11):337–339, 2000.

[9] C.N. Chuah, J.M. Kahn, and D.N.C. Tse. Capacity of multi-antenna arrays systems in indoor wireless environment. In *IEEE Global Telecommunications Conference*, pages 1894–1899, Sydney, Australia, 1998.

[10] D. Colton and R. Kress. *Inverse acoustic and elctromagnetic scattering theory*. Springer-Verlag, Berlin, 1992.

[11] R.K. Cook, R.V. Waterhouse, R.D. Berendt, S. Edelman, and J.R. Thompson. Measurement of correlation coefficients in reverberant sound fields. *Journal of the Acoustical Society of America*, 27(6):1072–1077, 1955.

[12] P.F. Driessen and G.J. Foschini. On the capacity formula for multiple-input multiple-output wireless channels: a geometric interpretation. *IEEE Transactions on Communications*, 47(2):173–176, 1999.

[13] G. J. Foschini and M. J. Gans. On limits of wireless communications in a fading environment when using multiple antennas. *Wireless Personal Communications*, 6(3):311–335, 1998.

[14] J. Fuhl, J.P. Rossi, and E. Bonek. High resolution 3-D direction-of-arrival determination for urban mobile radio. *IEEE Transactions on Antennas and Propagation*, 45:672–682, 1997.

[15] D. Gesbert, H. Bolcskei, D. Gore, and A. Paulraj. MIMO wireless channels: Capacity and performance prediction. In *IEEE Global Communications Conference*, San Francisco, USA, 2000.

[16] D. Gesbert, H. Bolcskei, D. Gore, and A. Paulraj. Outdoor mimo wireless channels: Models and performance prediction. *IEEE Transactions on Communications*, 50(12):1926–1934, 2002.

[17] D. Gesbert, T. Ekman, and N. Christophersen. Capacity limits of dense palm-sized MIMO arrays. In *IEEE Global Communications Conference*, Taipei, Taiwan, 2002.

[18] D. Gesbert, M. Shafi, D.S. Shiu, P. Smith, and A. Naguib. From theory to practice: An overview of MIMO space-time coded wireless systems. *IEEE Journal on Selected Areas in Communications, Special Issue on MIMO Systems*, 21(3):281–302, 2003.

[19] A. Gorokhov. Transmit diversity versus sdma: analytic and numerical comparisons. In *IEEE International Conference on Communications*, pages 1020–1024, New Orleans, LA, 2000.

[20] W.C. Jakes. *Microwave Mobile Communications*. John Wiley, New York, 1974.

[21] H.M. Jones, R.A. Kennedy, and T.D. Abhayapala. On dimensonality of multipath fields: spatial extent and richness. In *IEEE International Conference on Acoustics, Speech and Signal Processing*, Orlando, Florida, 2002.

[22] M. Kalkan and R.H. Clarke. Prediction of the space-frequency correlation function for base station diversity reception. *IEEE Transactions on Vehicular Technology*, 46:176–184, 1997.

[23] J.P. Kermoal, L. Schumacher, K.I. Pedersen, P.E. Mogensen, and F. Frederiksen. A stochastic mimo radio channel model with experimental validation. *IEEE Journal on Selected Areas in Communications*, 20(6):1211–1226, 2002.

[24] W.C.Y. Lee. Effects on correlation between two mobile radio base-station antennas. *IEEE Transactions on Vehicular Technology*, 22(4):130–140, 1973.

[25] W.C.Y. Lee. Finding the approximate angular probability density function of wave arrival by using a directional antenna. *IEEE Transactions on Antennas and Propagation*, 21:328–334, 1973.

[26] T. Lo and J. Litva. Angles of arrival of indoor multipath. *Electronic Letters*, 28:1687–1689, 1992.

[27] S. Loyka and A. Kouki. New compound upper bound on MIMO channel capacity. *IEEE Communications Letters*, 6(3):96–98, 2002.

[28] K.V. Mardia. *Statistics of Directional Data*. Academic Publishers, London, U.K., 1972.

[29] M. Patzold, U. Killat, Y. Li, and F. Laue. Modeling, analysis, and simulation of nonfrequency-selective mobile radio channels with asymmetrical doppler power spectral density shapes. *IEEE Transactions on Vehicular Technology*, 46(2):494–507, 1997.

[30] M. Patzold, L. Yingchun, and F. Laue. A study of a land mobile satellite channel model with asymmetrical doppler power spectrum and lognormally distributed line-of-sight component. *IEEE Transactions on Vehicular Technology*, 47(1):297–310, 1998.

[31] K.I. Pedersen, J.B. Anderson, J.P. Kermoal, and P.E. Mogensen. A stochastic multiple-input multiple-output radio channel model for evaluation of space-time coding algorithms. In *IEEE Vehicular Technology Conference*, pages 893–897, Boston, MA, 2000.

[32] K.I. Pedersen, P.E. Mogensen, and B.H Fleury. Power azimuth spectrum in outdoor environment. *IEE Electronic Letters*, 33(18):1583–1584, 1997.

[33] T.S. Pollock, T.D. Abhayapala, and R.A. Kennedy. Antenna saturation effects on dense array MIMO capacity. In *IEEE International Conference on Acoustics, Speech and Signal Processing*, pages 361–364, Hong Kong, 2003.

[34] J.P. Rossi, J.P. Barbot, and A.J. Levy. Theory and measurement of the angle of arrival and time delay of UHF radiowaves using a ring array. *IEEE Transactions on Antennas and Propagation*, 45(5):876–884, 1997.

[35] J.S. Sadowsky and V. Katedziski. On the correlation and scattering functions of the WSSUS channel for mobile communications. *IEEE Transactions on Vehicular Technology*, 47(1):270–282, 1998.

[36] J. Salz and J.H. Winters. Effect of fading correlation on adaptive arrays in digital mobile radio. *IEEE Transactions on Vehicular Technology*, 43(4):1049–1057, 1994.

[37] A.M. Sengupta and P.P. Mitra. Capacity of multivariate channels with multiplicative noise: I. random matrix techniques and large-n expansions fo full transfer matrices. Technical report, ATT Bell Labs, 2000.

[38] Da-Shan Shiu, G.J. Foschini, M.J. Gans, and J.M. Kahn. Fading correlation and its effect on the capacity of multielement antenna systems. *IEEE Transactions on Communications*, 48(3):502–513, 2000.

[39] Q. Spencer, M. Rice, B. Jeffs, and S.H. Jensen. A statistical model for angle of arrival in indoor multipath propagation. In *IEEE Vehicular Technology Conference*, pages 1415–1419, Phoenix, AZ, 1997.

[40] P.D. Teal, T.D. Abhayapala, and R.A. Kennedy. Spatial correlation for general distributions of scatterers. *IEEE Signal Processing Letters*, 9(10):305–308, 2002.

[41] E. Telatar. Capacity of multi-antenna gaussian channels. Technical report, ATT Bell Labs, 1995.

[42] E. Telatar. Capacity of multi-antenna Gaussian channels. *European Transactions on Telecommunications*, 10(6):585–596, 1999.

[43] J.A. Tsai, R.M. Buehrer, and B.D. Woerner. Spatial fading correlation function of circular antenna arrays with laplacian energy distribution. *IEEE Communications Letters*, 6(5):178–180, 2002.

[44] R.G. Vaughan. Pattern translation and rotation in uncorrelated source distributions. *IEEE Transactions on Antennas and Propagation*, 46(7):982–990, 1998.

[45] J.G. Wang, A.S. Mohan, and T.A. Aubrey. Angles-of-arrival of multipath signals in indoor environments. In *IEEE Vehicular Technology Conference*, pages 155–159, Atlanta, GA, 1996.

[46] S. Wei, D. Goeckel, and R. Janaswamy. On the capacity of fixed length antenna arrays under bandlimited correlated fading. In *Conference on Information Sciences and Systems*, pages 1088–1093, Princeton, 2002.

List of Figures

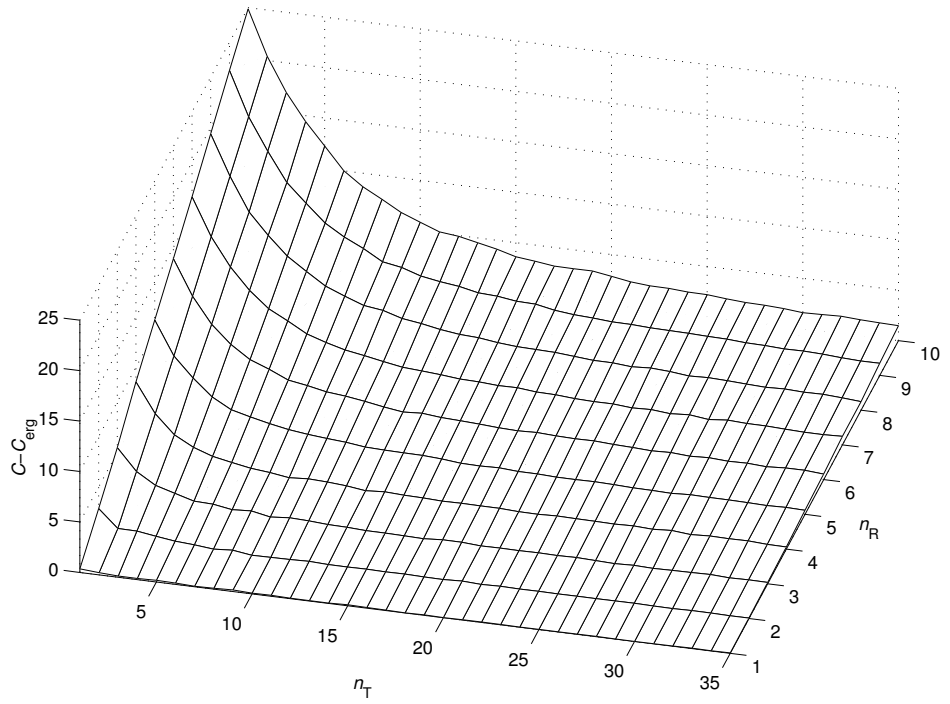

Figure 1: Convergence error of ergodic capacity C_{erg} (1) to bound C (5) with increasing number of transmit antennas for various numbers of receive antennas and SNR 10dB.

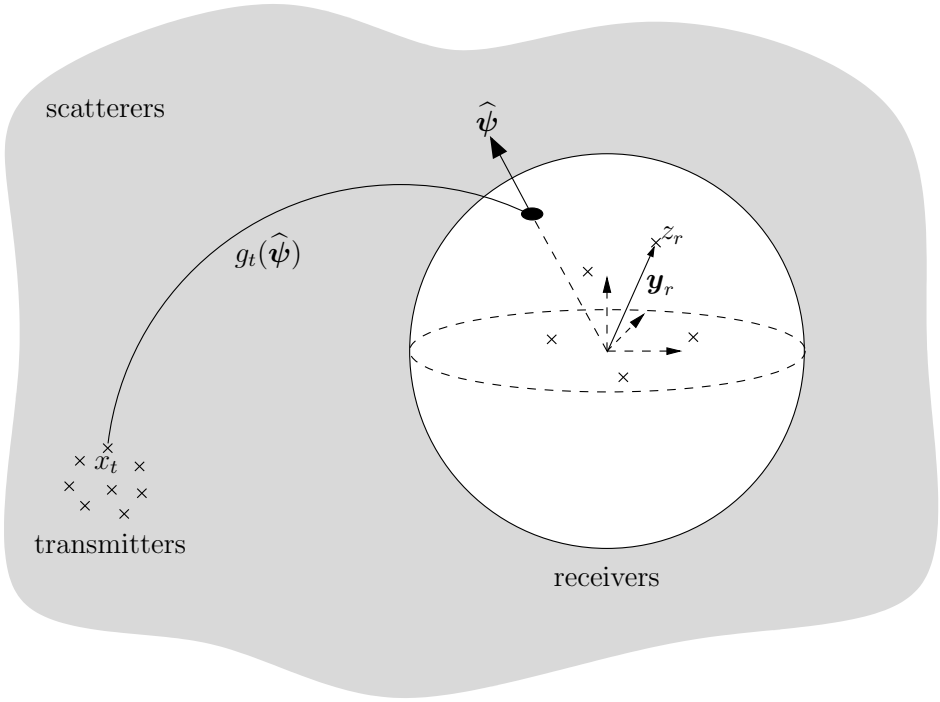

Figure 2: Scattering model for a flat fading MIMO system. $g_t(\widehat{\boldsymbol{\psi}})$ represents the effective random complex gain of the scatterers for a transmitted signal x_t arriving at the receiver array from direction $\widehat{\boldsymbol{\psi}}$ via any number paths through the scattering environment. The sphere surrounding the receive antennas contains no scatterers and is assumed large enough that any scatterers are farfield to all receive antennas located within.

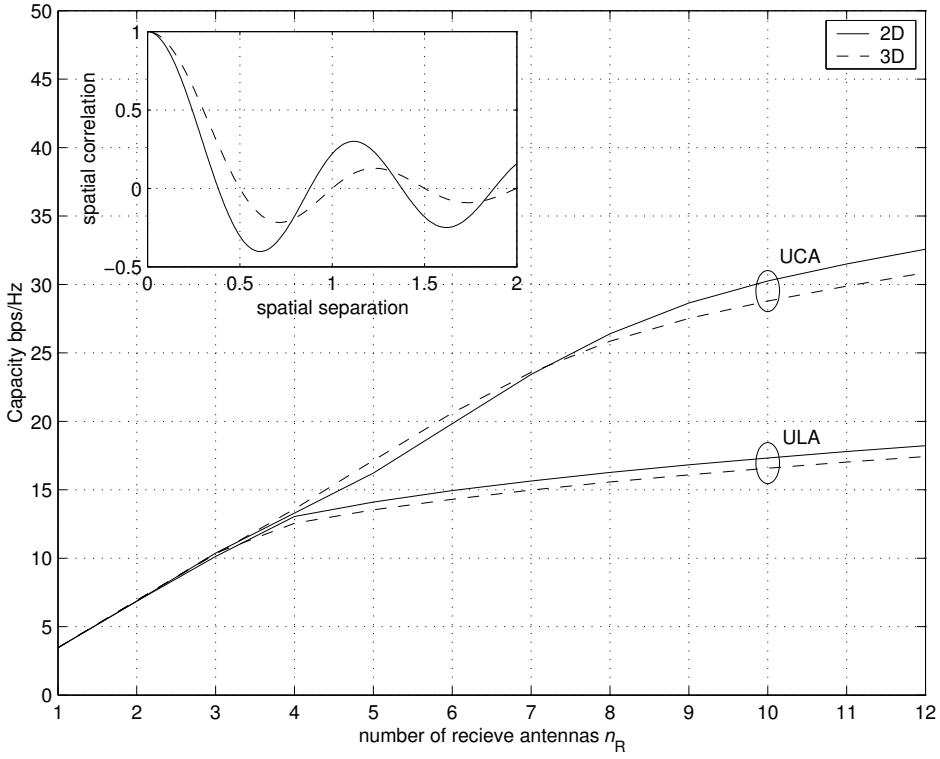

Figure 3: Capacity of 2D and 3D isotropic scattering environments for fixed length aperture (1λ) uniform linear (ULA) and uniform circular (UCA) arrays for increasing number of receive antennas. Insert: Spatial correlation between two antennas against spatial separation for the 2D and 3D isotropic scattering environments.

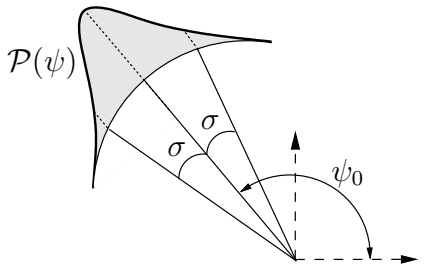

Figure 4: Multipath signal energy modelled as a non-isotropic scattering distribution $\mathcal{P}(\psi)$ with mean AOA ψ_0 and angular spread σ (defined as the standard deviation of the distribution).

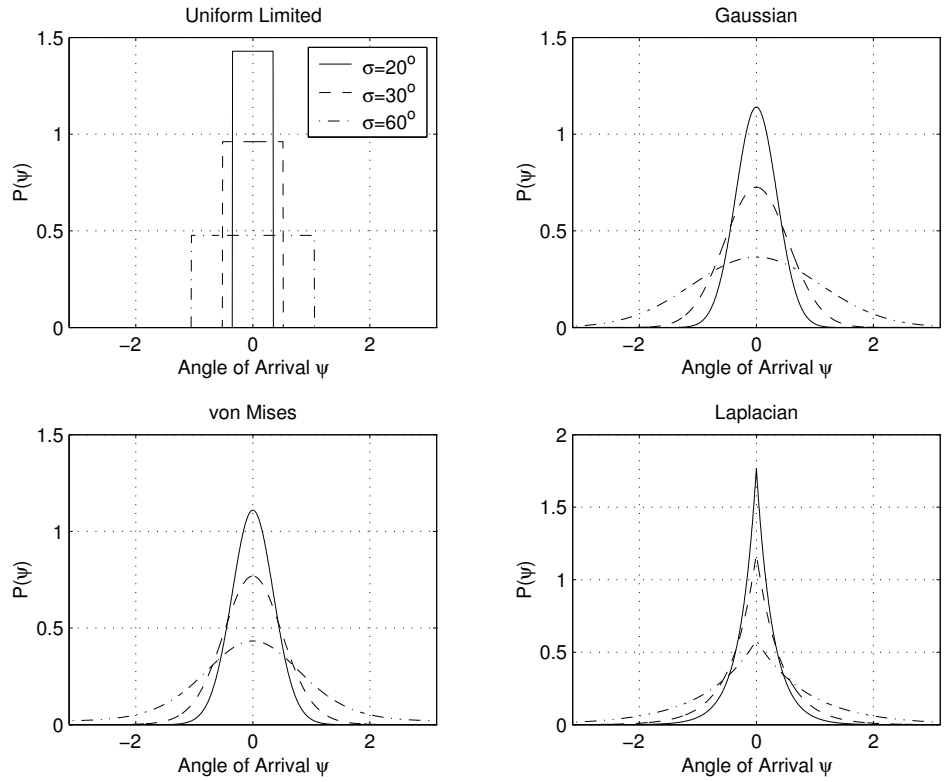

Figure 5: Comparison of common scattering distributions: Uniform, Gaussian, von-Mises and Laplacian, for angular spread $\sigma = \{20°, 30°, 60°\}$.

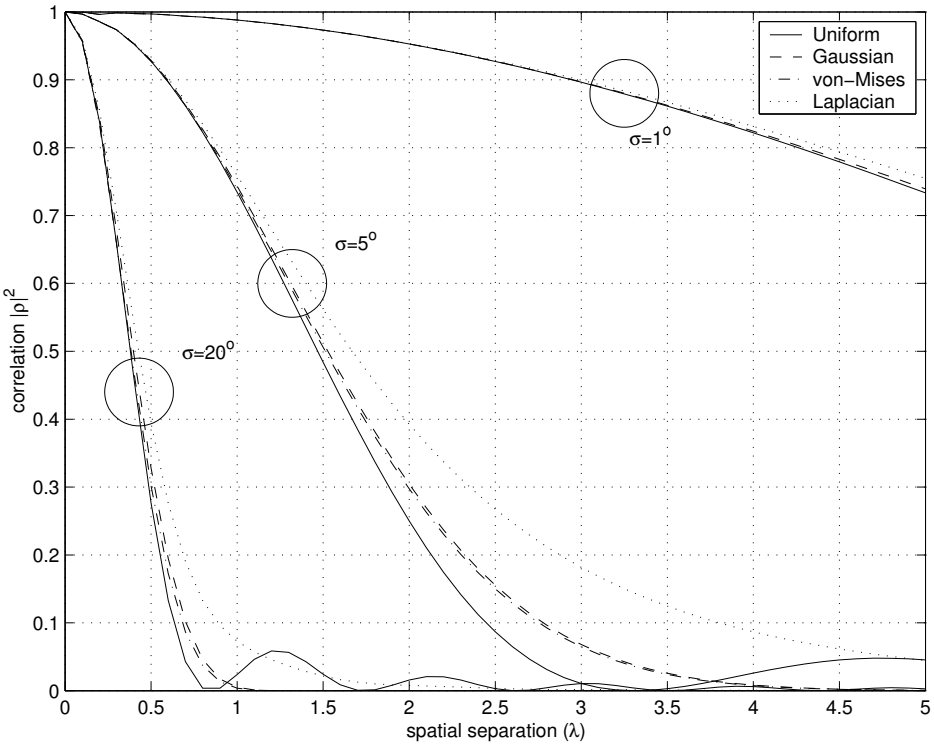

Figure 6: Spatial correlation between two antennas for mean AOA 90° (broadside) against spatial separation for Uniform, Gaussian, von-Mises, and Laplacian scattering distributions and angular spreads $\sigma = \{1°, 5°, 20°\}$.

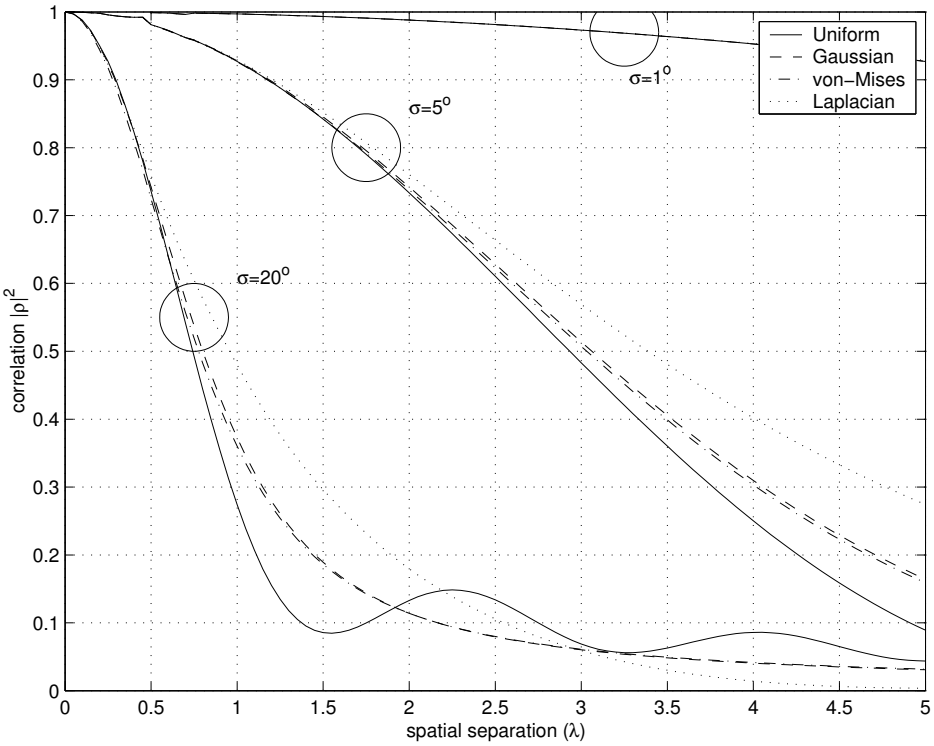

Figure 7: Spatial correlation between two antennas on the x-axis for mean AOA 30° (60° from broadside) against spatial separation for Uniform, Gaussian, von-Mises, and Laplacian scattering distributions and angular spreads $\sigma = \{1°, 5°, 20°\}$.

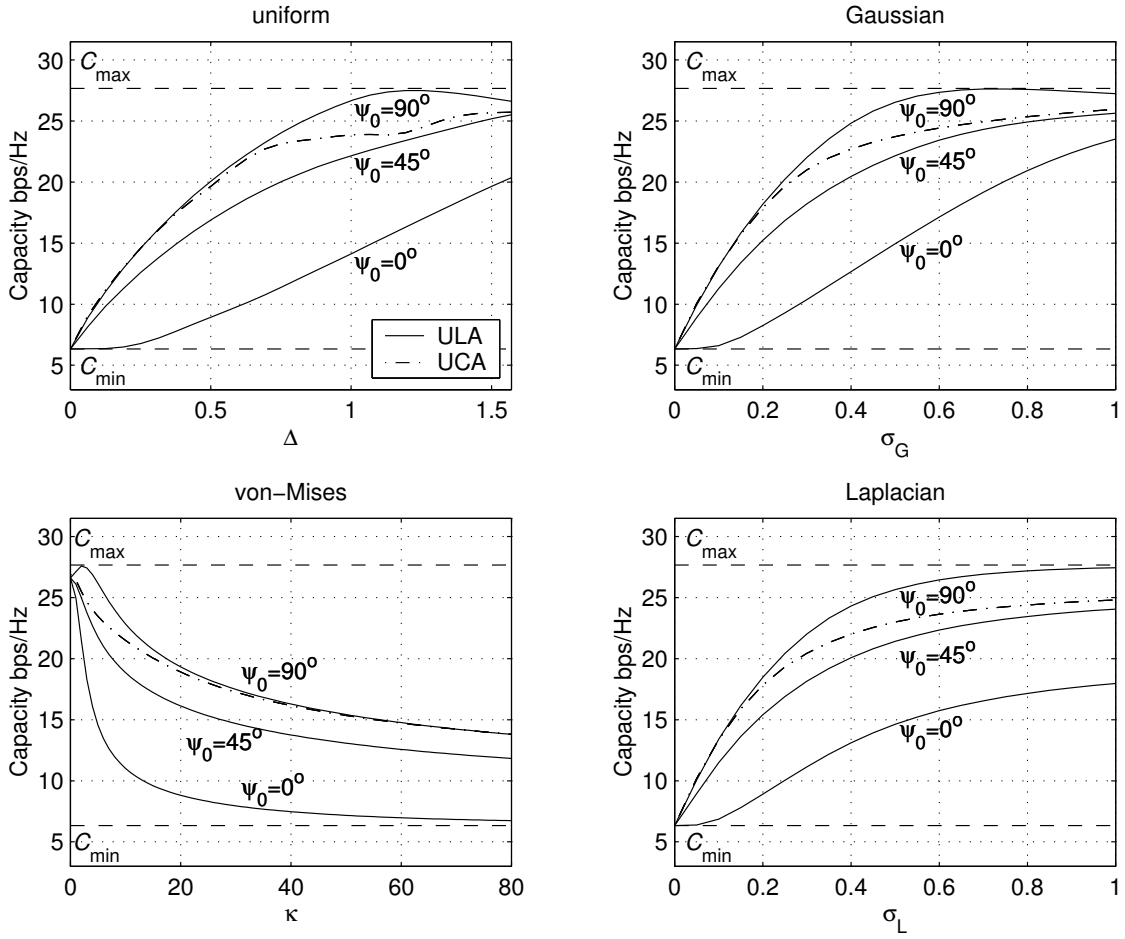

Figure 8: Capacity for non-isotropic distributed scattering with mean AOA $\psi_0 = \{0°, 45°, 90°\}$ and increasing nonisotropy factor, for the 8 antenna uniform linear (ULA) and uniform circular (UCA) arrays of aperture width (length/diameter) 3.5λ.

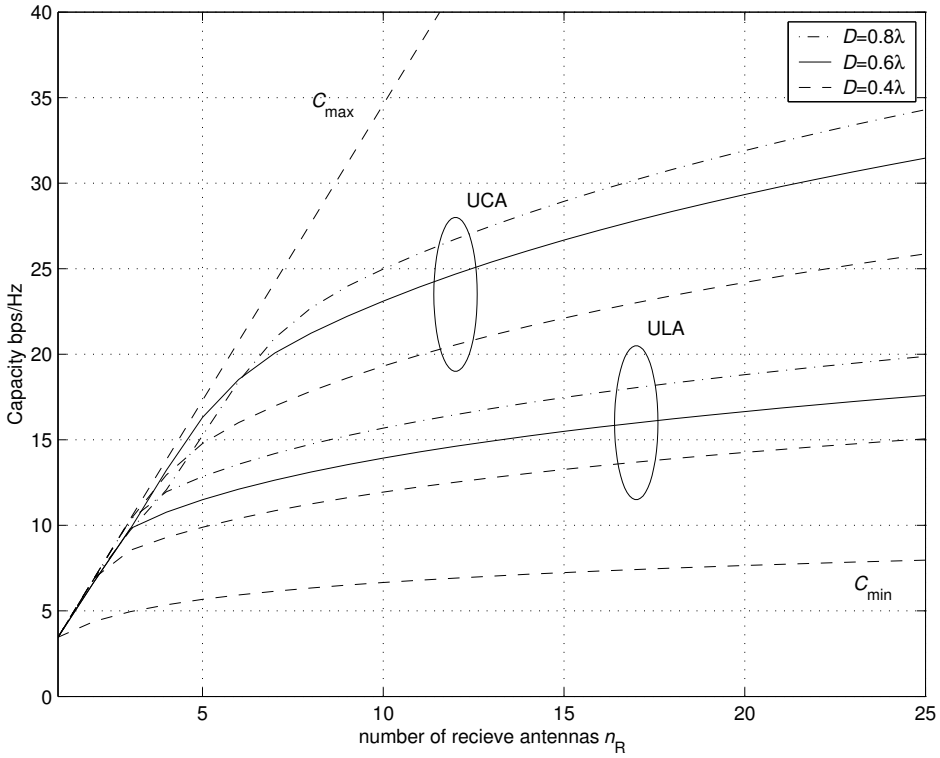

Figure 9: Capacity scaling of the uniform linear (ULA) and uniform circular (UCA) arrays with fixed aperture (length/diameter) $D = \{0.4\lambda, 0.6\lambda, 0.8\lambda\}$ in an isotropic scattering environment.

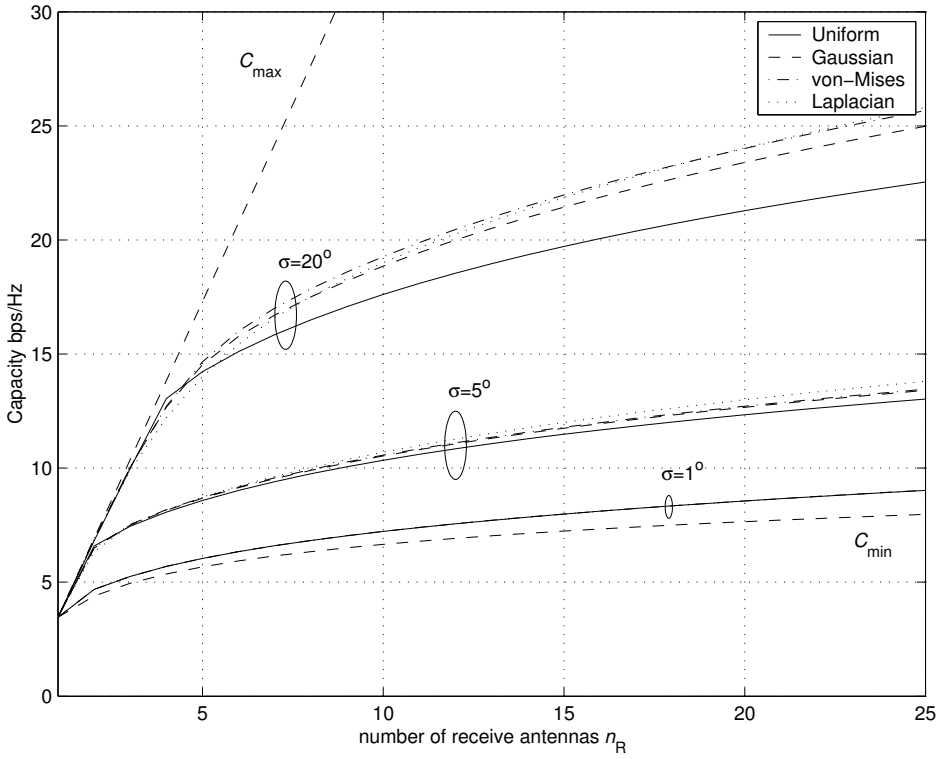

Figure 10: Capacity scaling of the broadside uniform linear array with fixed aperture 4λ for angular spread $\sigma = \{1°, 5°, 20°\}$ of the various scattering distributions.

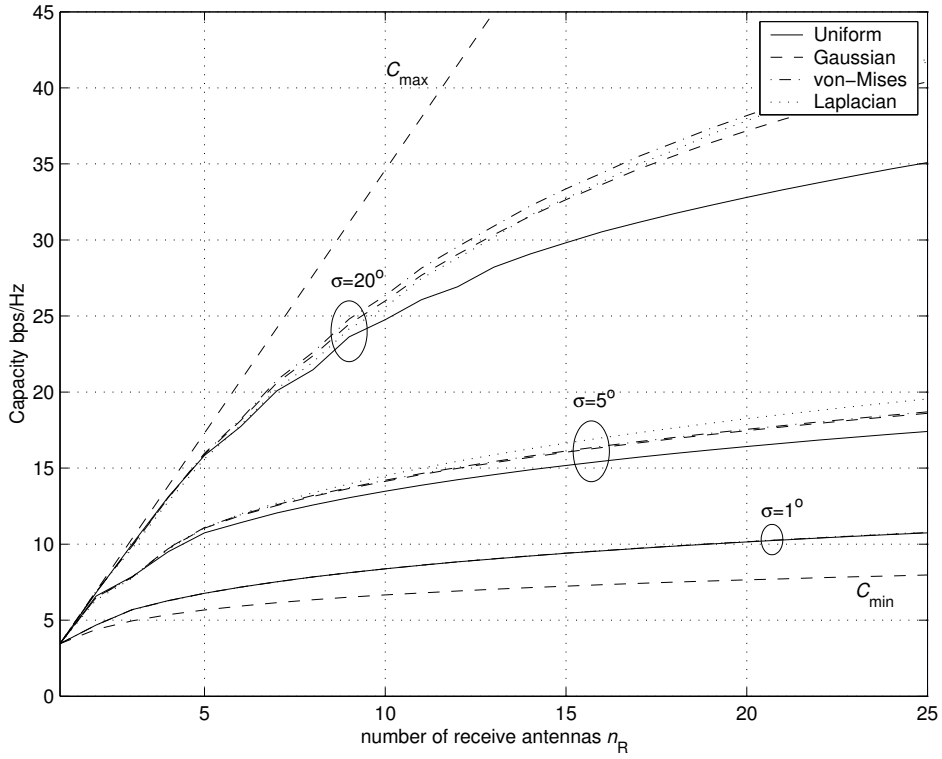

Figure 11: Capacity scaling of the uniform circular array with fixed aperture 4λ for angular spread $\sigma = \{1°, 5°, 20°\}$ of the various scattering distributions.

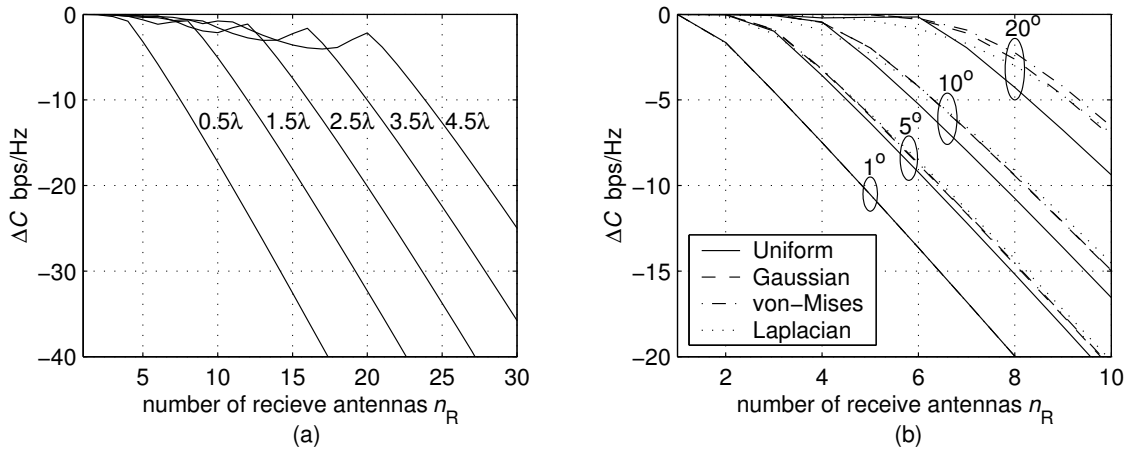

Figure 12: Capacity loss due to correlation of the broadside uniform linear array for: (a) fixed aperture $D = \{0.5\lambda, 1.5\lambda, 2.5\lambda, 3.5\lambda, 4.5\lambda\}$ in an isotropic scattering environment. (b) fixed aperture 4λ for angular spreads $\sigma = \{1°, 5°, 10°, 20°\}$ of the various scattering distributions.